Histidine Ligand Protonation and Redox Potential in the Rieske Dioxygenases: Role of a Conserved Aspartate in Anthranilate 1,2-Dioxygenase[†]

Zanna M. Beharry,[‡] D. Matthew Eby,[§] Eric D. Coulter,[‡] Rathinam Viswanathan,[‡] Ellen L. Neidle,[§] Robert S. Phillips,[‡] and Donald M. Kurtz, Jr.*[,‡]

Departments of Chemistry and Microbiology and Center for Metalloenzyme Studies, University of Georgia, Athens, Georgia 30602

Received August 5, 2003; Revised Manuscript Received September 29, 2003

ABSTRACT: The Rieske dioxygenase, anthranilate 1,2-dioxygenase, catalyzes the 1,2-dihydroxylation of anthranilate (2-aminobenzoate). As in all characterized Rieske dioxygenases, the catalytic conversion to the diol occurs within the dioxygenase component, AntAB, at a mononuclear iron site which accepts electrons from a proximal Rieske [2Fe-2S] center. In the related naphthalene dioxygenase (NDO), a conserved aspartate residue lies between the mononuclear and Rieske iron centers, and is hydrogen-bonded to a histidine ligand of the Rieske center. Engineered substitutions of this aspartate residue led to complete inactivation, which was proposed to arise from elimination of a productive intersite electron transfer pathway [Parales, R. E., Parales, J. V., and Gibson, D. T. (1999) *J. Bacteriol. 181*, 1831−1837]. Substitutions of the corresponding aspartate, D218, in AntAB with alanine, asparagine, or glutamate also resulted in enzymes that were completely inactive over a wide pH range despite retention of the hexameric quaternary structure and iron center occupancy. The Rieske center reduction potential of this variant was measured to be ∼100 mV more negative than that for the wild-type enzyme at neutral pH. The wild-type AntAB became completely inactive at pH 9 and exhibited an altered Rieske center absorption spectrum which resembled that of the D218 variants at neutral pH. These results support a role for this aspartate in maintaining the protonated state and reduction potential of the Rieske center. Both the wild-type and D218A variant AntABs exhibited substrate-dependent rapid phases of Rieske center oxidations in stopped-flow time courses. This observation does not support a role for this aspartate in a facile intersite electron transfer pathway or in productive substrate gating of the Rieske center reduction potential. However, since the single turnovers resulted in anthranilate dihydroxylation by the wild-type enzyme but not by the D218A variant, this aspartate must also play a crucial role in substrate dihydroxylation at or near the mononuclear iron site.

Rieske dioxygenases (RDOs),[1] also called aromatic ring-hydroxylating dioxygenases, are found in many species of soil bacteria, where they catalyze the initial step in aerobic degradation of a variety of aromatic compounds according to the transformation shown in Scheme 1. Both oxygen atoms of dioxygen are inserted into the aromatic ring, yielding

Scheme 1

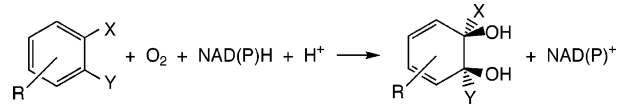

cyclic, nonaromatic *cis*-diols (*1*−*4*). A given RDO is typically specific for substrates having a set of closely related substituents, R, X, and Y.

All RDOs contain reductase and oxygenase components, the latter of which invariably contain both Rieske-type $[2Fe\text{-}2S]^{+}$ and mononuclear iron centers. The oxygenase component catalyzes the insertion of molecular oxygen into the aromatic substrate after receiving electrons from the reductase component (in some cases via an intervening ferredoxin). The insertion reaction requires activation of dioxygen, which apparently occurs when it binds to the ferrous mononuclear site followed by reduction of the $[Fe\text{-}O_2]^{2+}$ species by the Rieske center (*5*, *6*).

The X-ray crystal structure of the oxygenase component of the RDO, naphthalene dioxygenase (NDO), from *Pseudomonas* sp. NCIB 9816-4 (*7*), revealed a mushroom-shaped, three-fold rotationally symmetric $\alpha_3\beta_3$ hexamer, as shown in panels a and b of Figure 1. The distance between the

[†] This work was supported by National Institutes of Health Grant GM 59818 (E.L.N. and D.M.K.).

* To whom correspondence should be addressed. Phone: (706) 542-2016. Fax: (706) 542-9454. E-mail: kurtz@chem.uga.edu.

[‡] Department of Chemistry and Center for Metalloenzyme Studies.

[§] Department of Microbiology and Center for Metalloenzyme Studies.

[1] Abbreviations: RDOs, Rieske dioxygenases; NDO, naphthalene dioxygenase; AntDO, anthranilate 1,2-dioxygenase; AntAB, AntDO oxygenase component; AntA, AntAB α subunit; AntC, AntDO reductase component; BenDO, benzoate 1,2-dioxygenase; SDS−PAGE, sodium dodecyl sulfate−polyacrylamide gel electrophoresis; ICP-AE, inductively coupled plasma atomic emission; LB, Luria-Bertani medium; MOPS, 3-(*N*-morpholino)propanesulfonic acid; MES, 2-(4-morpholino)ethanesulfonic acid; HEPES, *N*-(2-hydroxyethyl)piperazine-*N*′-2-ethanesulfonic acid; CAPS, 3-(cyclohexylamino)propanesulfonic acid; TAPS, *N*-tris(hydroxymethyl)methyl-3-aminopropanesulfonic acid; apoAntAB, AntAB lacking the mononuclear site iron; DEANONOate, (*Z*)-1-(*N*,*N*-diethylamino)diazen-1-ium-1,2-diolate; NHE, normal hydrogen electrode; TLC, thin-layer chromatography; HPLC, high-performance liquid chromatography; EXAFS, extended X-ray absorption fine structure spectroscopy.

10.1021/bi035385n CCC: $25.00
Published on Web 10/30/2003

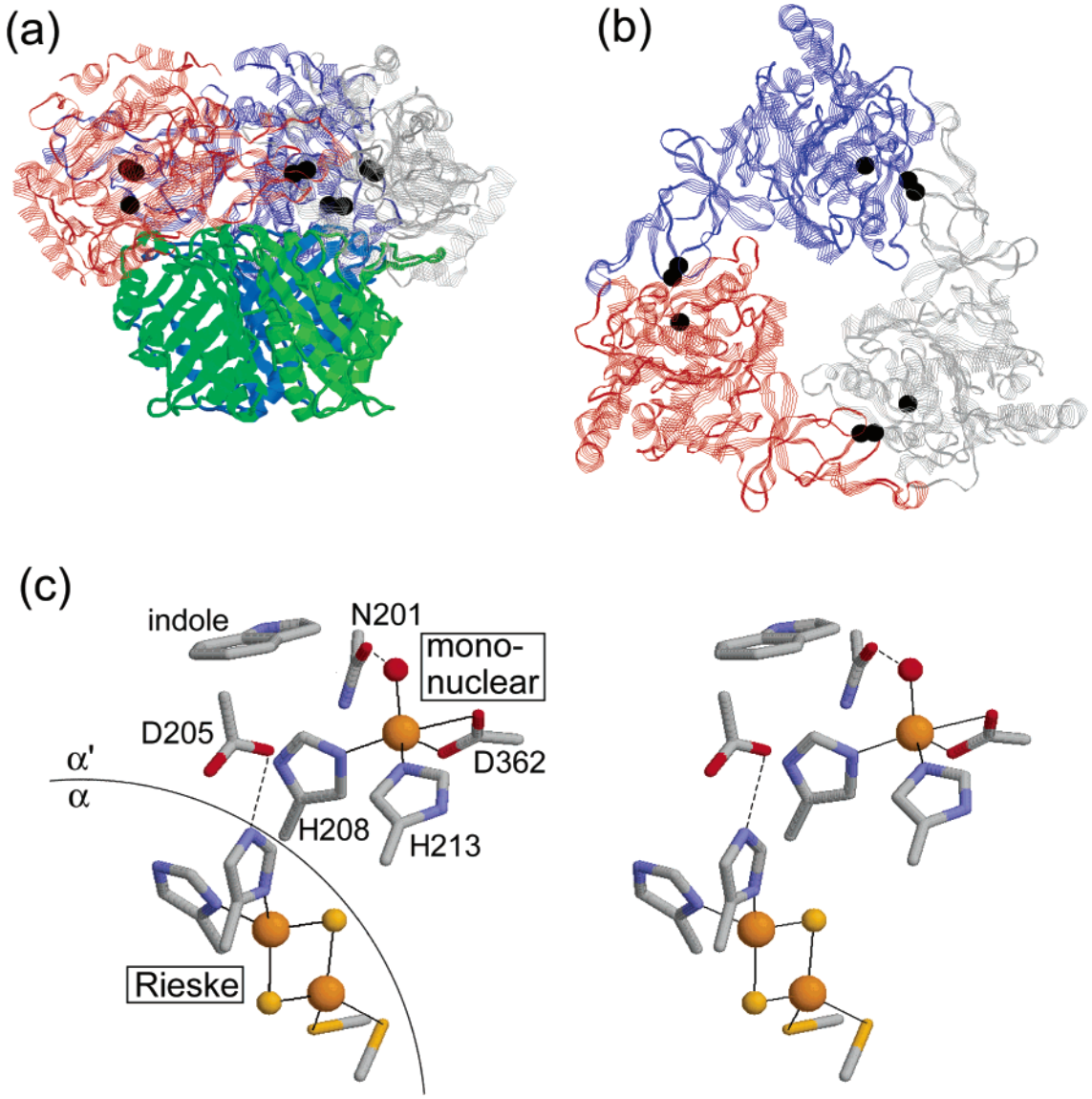

FIGURE 1: Structural features of NDO from *Pseudomonas* sp. strain NCIB 9816-4. (a) $\alpha_3\beta_3$ hexamer viewed perpendicular to the 3-fold rotational axis with α subunits (strand representation) on top and β subunits below (ribbon representation). (b) α_3 trimer within the hexamer viewed along the 3-fold rotational axis (protein backbone in ribbon representation). In both panels a and b, iron atom positions are represented by dark spheres, with paired spheres representing the Rieske center and single spheres representing mononuclear sites. (c) Stereoview of Rieske and mononuclear iron sites across an α−α′ subunit interface in a crystal soaked in indole, a substrate analogue. Only mononuclear site side chains are labeled to avoid crowding. Drawings were generated using RASMOL (*9*) and coordinates from Protein Data Bank entry 1eg9 (*10*).

Rieske and mononuclear iron centers within each α subunit is ~44 Å. A much shorter distance, ~12 Å, occurs between these two metal centers across adjacent α subunit interfaces (cf. panels b and c of Figure 1). This intersubunit route was, therefore, proposed to be the most efficient for the catalytically essential electron transfer between Rieske and mononuclear iron sites (*7*). The carboxylate of an aspartate residue, Asp205 in NDO (Figure 1c), was found to lie between the Rieske and mononuclear iron sites across each of the three α−α subunit interfaces and to be hydrogen-bonded to a ligand histidine of the Rieske center and, perhaps more weakly, to a histidine ligand of the mononuclear iron site. This aspartate residue is conserved in all known RDOs (*1*), and on the basis of its location and hydrogen bonding pattern in NDO, its carboxylate was proposed to constitute the major electron transfer pathway between the Rieske and mononuclear iron centers (*7*, *8*). Crude *Escherichia coli* extracts containing engineered NDO variants in which Asp205 was replaced with Ala, Glu, Asn, or Gln exhibited little or no ability to hydroxylate naphthalene and no ability to turn over substrate or dioxygen under conditions where the wild-type NDO extract did exhibit these activities (*8*). The Asp205Gln NDO variant was isolated and found to retain the native $\alpha_3\beta_3$ quaternary structure and functional Rieske center.

The soil bacterium *Acinetobacter* sp. strain ADP1 can use either anthranilate (2-aminobenzoate) or benzoate as the sole carbon source. Despite the structural resemblance of these substrates, this strain uses similar but distinct two-component RDOs, anthranilate 1,2-dioxygenase (AntDO) and benzoate 1,2-dioxygenase (BenDO), to catalyze the first steps of their respective degradations (*11*). These degradations and the enzyme components are diagrammed in Scheme 2 (labeled Ant/BenC and Ant/BenAB for the reductase and oxygenase components, respectively). Both substrates are converted to catechol, which is then degraded to tricarboxylic acid cycle intermediates via the β-ketoadipate (*ortho*) pathway (*12*).

Scheme 2

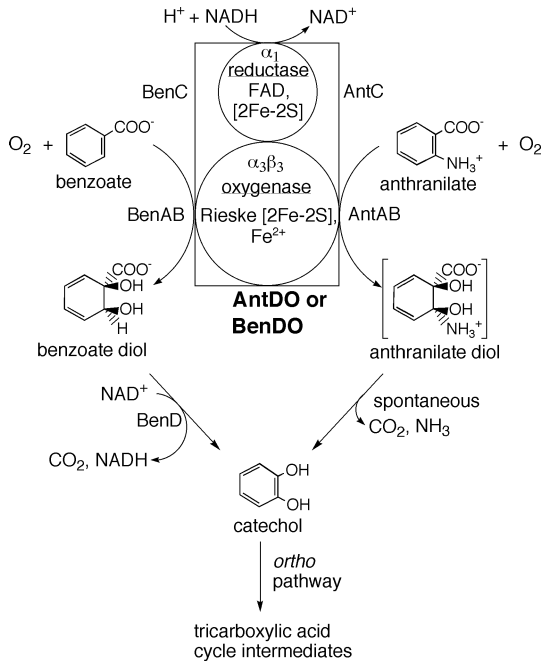

While benzoate catabolism uses an NAD^+-dependent dehydrogenase (BenD) for conversion to catechol, the putative anthranilate 1,2-diol produced by AntDO appears to spontaneously convert to catechol by loss of ammonia and carbon dioxide without the need for a dehydrogenase.

Although BenDOs were isolated and characterized from strain ADP1 (*12*) and from *Pseudomonas* strains several years ago (*13*, *14*), AntDO was only recently purified to homogeneity (*15*). The composition of the ADP1 AntDO oxygenase component, AntAB, mimicked that of NDO, i.e., an $\alpha_3\beta_3$ hexamer with one Rieske-type [2Fe-2S] center and one mononuclear iron site per α subunit. All residues contributing ligands to the Rieske and mononuclear iron sites of NDO [including Asn201 in the second coordination sphere (cf. Figure 1c)] are conserved in AntAB (*15*). Also conserved is the homologue to Asp205 in NDO, namely, Asp218 in the α subunit of AntAB. Herein, we report characterizations of engineered Asp218 variants of AntAB and provide evidence indicating a role for this conserved residue in modulating the protonation state and redox potential of the Rieske center, as well as in catalysis of aromatic ring dihydroxylation.

MATERIALS AND METHODS

Reagents and General Procedures. Anthranilate and ultrapure grade ammonium sulfate were purchased from Sigma Chemical Co. Oligonucleotides were synthesized by Integrated DNA Technologies. Nucleotide sequencing was performed at the University of Georgia Molecular Genetics Instrumentation Facility (Athens, GA) (ABI373 sequencer, Applied Biosystems). Protein purity was judged by sodium dodecyl sulfate−polyacrylamide gel electrophoresis (SDS−PAGE) (15% polyacrylamide gels) with Coomassie blue staining (*16*). Standard molecular biology procedures followed those by Sambrook et al. (*17*) or Ausubel et al. (*18*). Protein was quantitated using the Bio-Rad protein assay with bovine serum albumin as the standard. Native protein molecular weights (gel filtration) and iron quantitation (ferrozine method) were determined as previously described (*15*). Other metals in the proteins were quantitated by ICP-AE at the University of Georgia Chemical Analysis Laboratory (Athens, GA). For examination of the reduced Rieske center by EPR spectroscopy, excess sodium dithionite (~3 mM) was added to buffered AntDO samples that had been made anaerobic by purging with N_2 gas. The reduced samples were then transferred via a gastight syringe to EPR tubes that were continuously purged with N_2 gas and then frozen in liquid N_2.

Construction of D218 antAB Variants. Substitution of the aspartate 218 codon with that of alanine (D218A) in *antA* previously cloned from *Acinetobacter* sp. strain ADP1 (*11*) was carried out using the QuikChange site-directed mutagenesis kit (Stratagene) following the procedures described in the product manual. Plasmid pBAC209 (*11*), which contains *antAB*, was used as the template with the complementary mutagenic oligonucleotide primers 5′-GAAAATGGCCTCgctGGCTACCACGTC-3′ and 5′-GACGTGGTagcCAGCGAGGCCATTTTC-3′ (with the variant codon in lowercase), resulting in plasmid pDMK5. The D218N and D218E *antA* variants were constructed analogously, using mutagenic primer pairs 5′-GAAAATGGCCTCaatGGCTACCACGTC-3′ and 5′-GACGTGGTAGCCattGAGGCCATTTTC-3′ resulting in plasmid pDMK8 for D218N, and 5′-GAAAATGGCCTCgaaGGCTACCACGTC-3′ and 5′-GACGTGGTAGCCttcGAGGCCATTTTC-3′ resulting in plasmid pDMK9 for D218E. Successful substitution of the codons in all *antA* variant-encoding plasmids was verified by nucleotide sequencing.

Construction of an Acinetobacter Mutant Containing the D218A AntA Gene. The pDMK5 plasmid containing the D218A *antA* gene (designated as the *antA5476* allele) was digested with *Bgl*II. The resulting linearized plasmid was used as donor DNA in an *Acinetobacter* chromosomal allelic replacement method adapted from that of Neidle and Ornston (*19*). Cell lysates of resulting colonies that were ampicillin-sensitive and unable to grow with anthranilate as the sole carbon source were prepared, and *antA* was PCR-amplified therefrom using 29- and 42-base primers duplicating the nucleotide sequences of the 5′ and 3′ ends, respectively, of *antA*. Sequencing of the PCR amplicon confirmed the presence of the identical mutation in the chromosomal *antA5476* allele encoding D218A *antA* as found in pDMK5. The mutant ADP1 containing D218A *antA* in place of wild-type *antA* was designated strain ACN476.

Expression of Recombinant Enzymes in E. coli and Preparation of Cell-Free Extracts. Cultures (1 L) of *E. coli* strain BL21-Codon Plus (Stratagene) carrying pBAC208 (containing *antC*) (*15*), pBAC209 (*antAB*), pDMK5 (D218A *antAB*), pDMK8 (D218N *antAB*), or pDMK9 (D218E *antAB*) were grown aerobically in M9 minimal medium containing 100 mg/L ampicillin in an incubator/shaker at 37 °C until the OD_{600} reached ~0.6. The temperature was reduced to 30 °C, and ferrous ammonium sulfate (20 mg/L of culture) and isopropyl β-D-thiogalactoside (100 mg/L) were added. Incubation continued at this temperature until the OD_{600} reached ~2.5 (~4 h). Cells were harvested by centrifugation and washed with 25 mM MOPS at pH 7.3 (buffer A). Approximately 25 g of cells collected from 6 L of *E. coli* culture was resuspended in 25 mL of buffer A containing 1 mg of DNase and sonicated on ice using a model 350

Branson sonifier cell disrupter with a 0.5 in. probe tip for 2 min at 30 s intervals at 20 kHz. Cell debris was removed by centrifugation (12000*g* for 30 min at 4 °C). This preparation is termed the 6 × 1 L cell-free extract and was used immediately for isolation of the enzymes.

Isolation and Purification of Wild-Type and Variant AntABs. The procedure described below is modified from that described previously (*15*) and was used to isolate and purify both wild-type and D218 variant AntABs. All steps were carried out at 4 °C on the 6 × 1 L cell-free extracts. Column fractions containing AntAB were easily visualized by their red-brown color. The cell-free extract was applied to a 3 cm × 15 cm Q Sepharose FF anion exchange column (Amersham Pharmacia Biotech) equilibrated in buffer A. The column was washed with 200 mL of buffer A, and AntAB was eluted with a step gradient of NaCl (from 0 to 400 mM) in buffer A. Fractions containing AntAB were pooled, desalted, and concentrated by ultrafiltration to ∼2 mL (Amicon YM10 membrane). The concentrated mixture was applied to a 2 cm × 8 cm Mono Q anion exchange column (Amersham Pharmacia Biotech) equilibrated in buffer A. The column was washed with 50 mL of buffer A, and bound AntAB was eluted with a 250 mL linear gradient of NaCl (from 0 to 1 M) in buffer A. Fractions containing AntAB were pooled and concentrated by ultrafiltration to ∼2 mL and applied to a HiPrep 16/60 Sephacryl S300 column (Amersham Pharmacia Biotech) equilibrated in buffer A containing 250 mM NaCl. The column was eluted at a flow rate of 0.5 mL/min. The eluted fractions containing AntAB were pooled and concentrated by ultrafiltration (YM10 membrane) and stored at −80 °C in 100 μL aliquots. Approximately 15 mg of purified enzyme per liter of *E. coli* culture was obtained for both wild-type and D218 variant AntABs.

Purification of AntC. AntC was isolated from 6 × 1 L cell-free extracts at 4 °C under low-light conditions (to minimize loss of flavin) by a procedure modified from that described previously (*15*). Fractions containing AntC were readily visualized by their bright orange color. Anion exchange chromatography followed the same procedure described above for AntAB. Size exclusion chromatography was performed as described for AntAB using a HiPrep 16/60 Sephacryl S100 (Amersham Pharmacia Biotech) column. Purified AntC was dialyzed against buffer A containing 1 mM FAD (4 L for 12 h) and then dialyzed against buffer A (4 L for 12 h). The purified flavin-reconstituted AntC was concentrated by ultrafiltration (YM10 membrane) to ∼2 mL and stored at −80 °C. Approximately 12 mg of purified AntC was obtained per liter of *E. coli* culture.

Activity Assays. The concentrations of AntAB, D218A AntAB, and AntC were determined spectrophotometrically using published extinction coefficients for AntAB and AntC (*15*) and an ϵ_{454} of 14.9 mM^{-1} cm^{-1} for D218A AntAB determined in this work. The substrate-dependent O_2 and NADH consumption activities of wild-type and variant AntABs and AntC activities were measured as previously described (*15*). TLC was used to identify catechol produced in more concentrated AntDO assay mixtures: 30 μM in wild-type or variant AntAB $\alpha_3\beta_3$ combined with 5 μM AntC, 1 mM anthranilate, and 1 mM NADH in 50 mM MES and 100 mM KCl (pH 6.3). After incubation for 1 h at room temperature, the assay mixtures were spotted directly onto silica gel-coated glass TLC plates, which were then developed with a mobile phase of butanol, acetic acid, and water (4:1:4, v/v/v). Catechol was visualized on the TLC plates by staining the contents of the plates with 20% phosphomolybdic acid in ethanol (w/v). Catechol was also detected by reversed phase HPLC, as described previously (*15*).

Removal and Reconstitution of the Mononuclear Site Iron. Iron was removed from the mononuclear Fe(II) site by dialysis of either wild-type or D218A AntAB against buffer A containing 5 mM EDTA (4 L for 12 h) at 4 °C. The resulting wild-type or D218A apoAntAB was exchanged into buffer A by several concentration and redilution cycles in an Amicon concentrator. Iron and protein analyses, retention of the Rieske EPR signal, and loss of catalytic activity (for wild-type AntAB) were used to verify removal of only the mononuclear site iron. For reconstitution of the mononuclear site, the wild-type or D218A apoAntAB in buffer A was made anaerobic by purging with nitrogen gas. Nine-tenths to 1 molar equiv of Fe(II) or Co(II) per AntA mononuclear site (quantitated from the Bio-Rad protein assay) was added from anaerobic 10 mM stock solutions of ferrous ammonium sulfate or cobaltous chloride.

Nitric Oxide Adducts of AntAB and D218A AntAB. All steps were carried out using anaerobic solutions and gastight syringes. Iron-reconstituted wild-type or D218A AntAB in buffer A was divided into two portions, and anthranilate from an anaerobic stock solution was added to a final concentration of 1 mM to one portion. Diethylammonium (*Z*)-1-(*N*,*N*-diethylamino)diazen-1-ium-1,2-diolate (DEANONOate) (Cayman Chemicals) from a 25 mM stock solution in 0.01 M NaOH was added to both portions to a final concentration of 1 mM. DEANONOate is stable at high pH but decomposes to release NO gas at pH ∼7. The samples were incubated for ∼30 min before being transferred via a gastight syringe to EPR tubes and frozen in liquid nitrogen.

Stopped-Flow Spectrophotometry. Buffer solutions were vacuum degassed by flushing them with nitrogen gas and then transferred to a Coy anaerobic chamber along with the stopped-flow syringes, where they were washed with a dilute sodium dithionite solution and then washed thoroughly with anaerobic buffer A. Protein and stock anthranilate solutions were also prepared in the anaerobic chamber. The AntAB samples were added to quartz cuvettes in the chamber, and the cuvettes were sealed with a rubber septum and then removed from the chamber. Nitrogen gas was passed over the surface of the AntAB solutions in the cuvettes by piercing the rubber septum with a syringe needle, and reagents were added via a gastight syringe. Reduction of either wild-type (12 μM $\alpha_3\beta_3$) or D218A (16 μM $\alpha_3\beta_3$) apoAntAB in ∼2 mL of buffer A was accomplished by careful anaerobic spectrophotometric titration with NADH in the presence of 0.1 μM AntC. The titrations were continued until the spectra of reduced AntAB or D218A AntAB were reached and no additional absorbance at 340 nm was observed due to excess NADH. Where appropriate, anthranilate was added to a final concentration of 0.2 mM, and/or 1 molar equiv of iron(II) or cobalt(II) was added to reconstitute empty mononuclear sites. The reduced AntAB samples were transferred via a gastight syringe (that had been washed with anaerobic buffer) into the prewashed syringe on the stopped-flow spectrophotometer. The other stopped-flow syringe was loaded with an equal volume of O_2-saturated buffer A. Stopped-flow

Table 1: Properties of Recombinant *Acinetobacter* sp. ADP1 AntAB and D218 Variants[a]

AntAB	molecular mass (kDa)		irons/protein[b]	UV−vis (nm) (ϵ, mM^{-1} cm^{-1})[b]	Rieske$_{red}$ EPR *g* values	specific activities[d]	
	SDS−PAGE	gel filtration				NADH consumed	O_2 consumed
wild-type	52 (α) 24 (β)	220	8.8 ± 1.0	320 (31), 454 (14.4), 555 (7)	2.01, 1.93, 1.80	38 ± 2	40 ± 1
D218A	52 (α) 24 (β)	220	9.2 ± 0.7	320 (36) 419 (17.6) 454 (14.9) 474 (16), 555 (9.6)	2.01, 1.93, 1.80	0	0
D218N	52 (α) 24 (β)	220	8.7 ± 0.7	ND[c]	ND[c]	0	0
D218E	52 (α) 24 (β)	220	5.8 ± 1.2	ND[c]	ND[c]	0	0

[a] Data from this work, except for those for wild-type AntAB, which are taken from Eby et al. (*15*). [b] Per $\alpha_3\beta_3$, as isolated. [c] Not determined. [d] Assay conditions: 100 μM NADH, 250 μM O_2, 500 μM anthranilate, 0.5 μM AntAB $\alpha_3\beta_3$, and 0.18 μM AntC, in 50 mM MES and 100 mM KCl (pH 6.3) at room temperature (~23 °C). NADH consumption activity was monitored as ΔA_{340}. O_2 consumption was monitored with a Clark-type O_2 electrode; activities are reported as micromolar NADH or O_2 consumed per minute per micromolar AntAB $\alpha_3\beta_3$ and are the averages of three determinations.

spectrophotometry was performed on an RSM 1000 rapid-scanning spectrophotometer with a photomultiplier detector (OLIS Inc., Bogart, GA). Following stopped-flow mixing, the time dependences of the absorption spectra were monitored between 400 and 600 nm, and the data were analyzed using software supplied by OLIS Inc. Spectra of reduced AntAB shot against anaerobic buffer A in place of the O_2-satuated buffer showed that the protein had remained reduced during loading and verified that no anaerobic reaction occurred following mixing.

Redox Potential Measurements. Reduction potentials of the Rieske centers of wild-type and D218A AntABs were measured by spectrophotometric, dye-mediated, electrochemical titrations. A platinum/glass combination microelectrode (Brinkmann, Inc.) attached to a potential meter (World Precision Instruments, Inc.) was inserted through a tight-fitting rubber septum into a specially designed quartz cuvette containing 4 mL of anaerobic solution under an argon atmosphere. The solution contained ~30 μM wild-type or D218A AntAB hexamer ($\alpha_3\beta_3$) in 50 mM MOPS (pH 7.0) and each of the following redox dyes at 0.5 μM (reduction potentials, $E^{\circ\prime}$, vs SHE): methyl viologen (−446 mV), phenosafranine (−244 mV), anthraquinone-2,6-disulfonate (−184 mV), indigo carmine (−120 mV), indigo trisulfonate (−75 mV), indigo tetrasulfonate (−38 mV), methylene blue (8 mV), toluidine blue (34 mV), and phenazine methosulfate (92 mV) (*20*). Into these solutions were injected small aliquots (1−10 μL) of a concentrated stock solution of sodium dithionite in the same buffer. Stepwise reoxidation was achieved by injecting small aliquots (~5 μL) of air. After each addition, thorough mixing, and equilibration (which required ~10 min after mixing), the potential and UV−visible absorption spectra were recorded. The electrode was calibrated and referenced to the NHE by performing similar electrochemical titrations on and using the published reduction potentials versus NHE of *Desulfovibrio vulgaris* rubredoxin (0 mV) (*21*, *22*) and horse heart cytochrome *c* (254 mV) (*23*).

Other Spectroscopies. EPR spectra were recorded on a Bruker ESP-300E spectrometer equipped with an ER-4116 dual-mode cavity and an Oxford Instruments ESR-9 flow cryostat. Ultraviolet−visible absorption spectra were obtained in 1 cm path length quartz cuvettes on a Shimadzu UV-2401PC scanning spectrophotometer.

RESULTS

Acinetobacter ADP1-Derived Mutant Containing a D218A-Encoding antA Gene. The ACN476 mutant, in which the D218A-encoding allele replaced the wild-type *antA*, grew in a manner identical to that of the wild-type ADP1 strain on succinate minimal medium (*24*) at either 37 °C or room temperature. However, unlike the wild type, this mutant failed to grow at either temperature on anthranilate minimal medium (*19*) in either liquid cultures or agar plates. ACN476 was able to grow with benzoate as the sole carbon source, demonstrating that the genes required for degradation of catechol via the β-ketoadipate pathway are functional in this mutant.

Purification and Characterization of Wild-Type and D218 Variant AntABs. As noted previously (*15*), expression of enzymatically active recombinant *Acinetobacter* AntAB in *E. coli* could be qualitatively detected as gradual formation of the purple iron−catechol complex in cultures containing added anthranilate (~2 mM) and ferrous iron. Apparently, an *E. coli* reductase is able to supply electrons to AntAB for this conversion in the absence of its native reductase component, AntC. No such color change was observed in cultures of *E. coli* BL21-Codon Plus[pDMK5], -[pDMK8], or -[pDMK9] expressing the D218A, -N, or -E variant AntAB, respectively. Despite the apparent lack of AntDO activity, the D218 variant AntABs could be purified from these *E. coli* cultures in yields similar to that for the recombinant wild-type AntAB.

Table 1 compares the properties of purified wild-type and D218 variant AntABs. Size exclusion chromatography of purified D218A, -N, and -E AntABs gave molecular masses indistinguishable from that of wild-type AntAB, i.e., ~220 kDa, indicating that the D218 variants retained the $\alpha_3\beta_3$ hexameric quaternary structure. Iron analyses of D218A and D218N AntAB showed ~9 Fe atoms per $\alpha_3\beta_3$ (cf. Table 1), indicating full occupancy of the Rieske and mononuclear sites by iron, as was found for the recombinant wild-type AntAB (*15*). Iron analysis of D218E AntAB gave ~6 Fe atoms per $\alpha_3\beta_3$, which, together with the UV−vis absorption spectrum showing an intact Rieske center, indicates that the mononuclear sites were not occupied by iron in this variant. Neither the wild type nor any of the D218 variant AntABs contained other transition metals in molar ratios exceeding 0.2 metal atom per $\alpha_3\beta_3$, as determined by ICP-AE. D218A

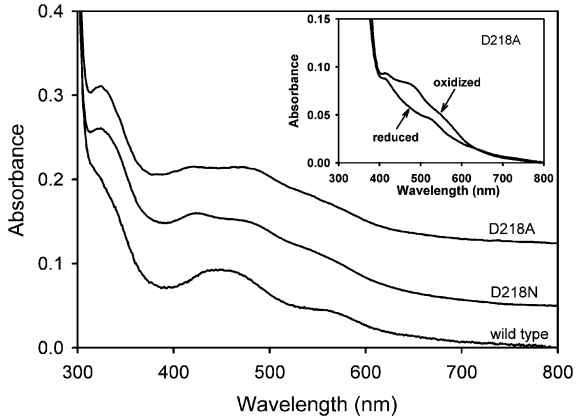

FIGURE 2: UV−visible absorption spectra of wild-type (7 μM α_3), D218A (6 μM $\alpha_3\beta_3$), and D218N (7 μM $\alpha_3\beta_3$) AntABs all in buffer A. Spectra are offset vertically for clarity. In the inset are shown UV−visible absorption spectra of oxidized D218A AntAB (6 μM, $\alpha_3\beta_3$) with 50 μM NADH in buffer A and the same mixture after addition of 1 μM AntC to catalyze reduction of D218A AntAB; absorption features below 400 nm are obscured by the absorbance of NADH. The reduction was performed anaerobically.

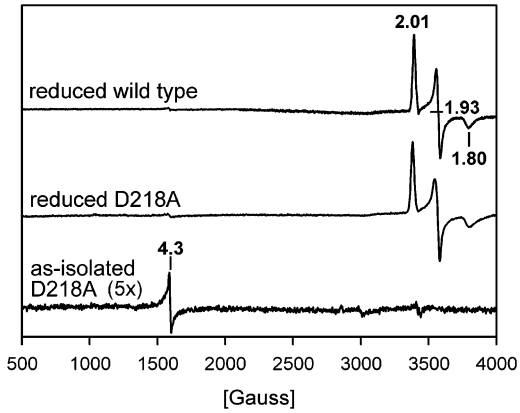

FIGURE 3: EPR spectra of (from top to bottom) dithionite-reduced wild-type AntAB (250 μM $\alpha_3\beta_3$), dithionite-reduced D218A AntAB (200 μM $\alpha_3\beta_3$), and as-isolated D218A AntAB (200 μM $\alpha_3\beta_3$) all in buffer A. Samples were prepared as described in Materials and Methods. EPR conditions: temperature, 10 K; microwave frequency, 9.60 GHz; modulation amplitude, 6.366 G; and microwave power, 2 mW.

AntAB was the most thoroughly studied of the variants. Unlike the wild-type protein, minor portions of D218A AntAB samples underwent irreversible precipitation upon freezing and thawing. Removal of the precipitate by centrifugation gave a supernatant with spectral properties unaltered from those obtained prior to freezing. Typically, fresh (unfrozen) preparations of D218 variant AntABs were used for the experiments described below.

Spectroscopic Properties of D218 Variant AntABs. The near-UV−visible absorption spectra of the as-isolated wild-type and D218 variant AntABs are shown in Figure 2. The visible absorption spectrum of wild-type AntAB is due to the oxidized ([2Fe-2S]$^{2+}$) Rieske center. In the corresponding spectra of D218A and -N AntAB, the broad absorption maximum of wild-type AntAB at ~454 nm has partially resolved into two features with maxima at ~419 and ~474 nm. In addition, the shoulders at ~320 and ~550 nm of the wild-type AntAB spectrum have become better and less well defined, respectively, in the D218 variant AntAB spectra. Similar absorption spectral perturbations were found for the D218E variant (not shown). Addition of ferricyanide to the as-isolated D218A AntAB did not result in any changes in the absorption spectrum of the Rieske center, indicating that the spectral perturbation relative to the wild type is not due to partial reduction of the Rieske center. Also, the EPR spectrum of as-isolated D218A AntAB (Figure 3) (without any added reducing or oxidizing agents) showed essentially no signal from the reduced Rieske center, but did show a $g = 4.3$ signal due to mononuclear high-spin ferric iron. The intensity of this signal corresponds to at most only a few percent of the mononuclear iron sites in the sample (*25*), and this weak signal may be due to adventitiously bound high-spin ferric iron.

As shown in the inset of Figure 2, the Rieske center of D218A AntAB could be reduced anaerobically with a catalytic amount of AntC and excess NADH, resulting in a spectrum with significantly decreased absorption between 400 and 600 nm, and which closely resembles that of reduced ([2Fe-2S]$^{+}$) wild-type AntAB (*15*). Essentially identical absorption spectral changes (not shown) occurred for D218N and -E AntABs when they were anaerobically treated with the same amounts of NADH and AntC. These results (and EPR spectra of NADH/AntC-reduced D218A AntAB discussed below) demonstrate that electron transfer from AntC to the AntAB Rieske centers remains intact in the D218 variants. The 10 K EPR spectrum of dithionite-reduced D218A AntAB (Figure 3) showed *g* values identical to those of reduced wild-type AntAB at 2.01, 1.93, and 1.80, which are characteristic of Rieske-type [2Fe-2S]$^{+}$ centers. Thus, substitution of aspartate 218 perturbs the visible absorption spectrum of the oxidized Rieske site in AntAB, whereas neither the visible absorption nor EPR spectra of the reduced Rieske center were detectably perturbed. None of the visible absorption spectra of wild-type or variant AntABs were affected by the addition of excess anthranilate.

pH Dependence of the Oxidized Rieske Center Absorption Spectrum. The perturbation of the oxidized Rieske center absorption spectrum in the D218 variant AntABs (cf. Figure 2) is reminiscent of that occurring upon exposure of Rieske ferredoxins to basic pHs (*26*). We, therefore, examined the pH dependence of the absorption spectrum of wild-type AntAB with an oxidized Rieske center. Figure 4 shows the perturbation of the Rieske absorption spectrum of AntAB when the pH is increased from 6 to 9. Over the course of ~10 min, the shoulder at ~555 nm became less prominent and the single broad peak at ~454 nm split into two peaks at ~420 and 470 nm. Comparison with the spectra in Figure 2 shows that the absorption spectrum of oxidized wild-type AntAB at pH 9 more closely resembles that of the D218 variant AntABs obtained at pH 7.3. This behavior is consistent with an ionizable proton at or near the Rieske center, the pK_a of which is lowered in the D218A variant.

Effect of the D218A Mutation on the Redox Potential of the AntAB Rieske Center. The aspartate 218 to alanine replacement made the AntAB Rieske center reduction potential significantly more negative. Figure 5 shows Nernst plots resulting from electrochemical titrations of wild-type and D218A AntABs. The least-squares fits to the data resulted in midpoint reduction potentials of -86 ± 10 and -187 ± 10 mV versus NHE at pH 7 for the wild-type and D218A Rieske centers, respectively. The wild-type AntAB

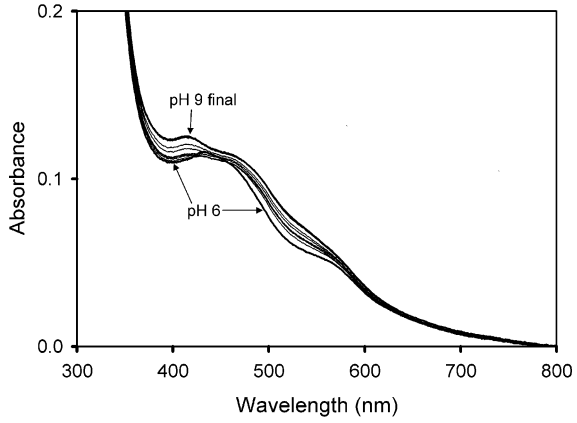

FIGURE 4: Visible absorption spectra of wild-type AntAB diluted from a concentrated stock to 8 μM $\alpha_3\beta_3$ with buffer at either pH 6 (bottom thick trace) or pH 9. The top thick trace was recorded 10 min after dilution into the pH 9 buffer. Thinner traces represent spectra recorded between 0 and 10 min after dilution into the pH 9 buffer. The buffer, at a total concentration of 50 mM, consisted of equimolar MES, MOPS, HEPES, CAPS, and TAPS adjusted to either pH 6 or 9.

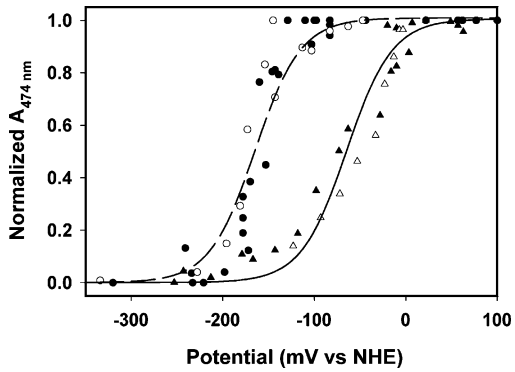

FIGURE 5: Nernst plots of the fractional absorbance at 474 nm vs solution potential for wild-type (triangles) and D218A (circles) AntAB. Data were obtained at room temperature in 50 mM MOPS (pH 7.0), as described in Materials and Methods. Empty symbols are for titrations starting from oxidized protein and filled symbols starting from dithionite-reduced protein. All data points from three independent titrations of each protein are plotted. Solid curves are least-squares fits of the Nernst equation to the cumulative data for each protein, assuming a one-electron process, yielding the midpoint potentials listed in the text.

Rieske center reduction potential falls within the range of those reported for other RDO oxygenase components (−50 to −150 mV vs NHE) (*27*−*31*). The D218A AntAB Rieske center reduction potential, however, is lower than that reported for any other RDO.

Activities of D218 Variant AntABs. Activities of the D218 variant AntABs were measured by monitoring the anthranilate-dependent oxidation of NADH under conditions previously optimized for wild-type AntAB (*15*). The conversion of anthranilate to catechol by wild-type AntDO under these assay conditions is a tightly coupled two-electron process in which NADH, O_2, and anthranilate are consumed to form catechol in a 1:1:1:1 molar stoichiometry, as expected for AntDO-catalyzed reaction 1 (cf. Scheme 2). Under these conditions, wild-type AntAB oxidized 40 μmol of NADH min^{-1} (μmol of AntAB $\alpha_3\beta_3)^{-1}$, but none of the D218 AntAB variants (D218A, -N, or -E) showed any detectable NADH consumption, O_2 consumption, or catechol formation, i.e., no evidence of anthranilate dioxygenase activity. The D218 AntAB variants also failed to catalyze NADH consumption when anthranilate was omitted from the standard assay mixture; i.e., these variants also exhibited no uncoupled NADH oxidase activity. The absorption spectra in the inset of Figure 2 verify that this lack of activity is not due to an inability of AntC to reduce the Rieske centers of D218A AntAB. Addition of ferrous iron (100 μM) did not stimulate any NADH oxygenase or oxidase activity of the mutated AntABs in the presence or absence of anthranilate, respectively. D218A AntAB activity assays conducted with the standard enzyme and reagent concentrations (cf. Materials and Methods) at pH 5.5, 6, 6.5, 7, 8, and 9 also showed no NADH consumption. Solutions containing up to 30 μM D218A AntAB $\alpha_3\beta_3$, catalytic AntC, and excess NADH at pH 6.3 (optimal for wild-type AntAB activity) showed no catechol formation when reaction mixtures were either spotted onto TLC plates after incubation for ~1 h at room temperature or analyzed by reversed phase HPLC (*15*). Under analogous single-turnover conditions, catechol could be readily detected for wild-type AntAB by both TLC and HPLC.

Nitrosyl Adducts of Wild-Type and D218A AntAB Mononuclear Sites. To probe O_2 and substrate access to the mononuclear Fe(II) site, nitric oxide adducts of the wild-type and D218A AntAB mononuclear iron sites were generated in both the presence and absence of anthranilate. Nitric oxide has been employed as an O_2 mimic in other RDOs, where it reacts with mononuclear ferrous centers to yield EPR-active $S = {}^3/_2$ $[FeNO]^7$ complexes (*25*, *32*). Prior to formation of the NO adducts, iron was removed from the mononuclear sites of both wild-type and D218A AntABs by dialysis against EDTA, yielding the apoAntABs. The enzymes were then reconstituted by anaerobic addition of 0.9 molar equiv of ferrous iron. This iron removal and reconstitution procedure was performed to minimize the EPR resonance at $g = 4.3$ due to ferric ions in the as-isolated oxygenase (cf. Figure 3). Figure 6 (top spectrum in each panel) shows that reconstitution of apoAntAB or apoD218A AntAB with Fe(II) followed by anaerobic exposure to NO yielded adducts showing EPR signals near $g = 4$ (bottom spectrum in each panel), consistent with the expected $S = {}^3/_2$ species, and a weak residual Fe(III) signal at $g = 4.3$. The addition of anthranilate induced the appearance of distinctly rhombic $S = {}^3/_2$ spectral components near $g = 4$ (bottom spectrum in each panel of Figure 6). At least two such substrate-perturbed spectral components were observed for the wild-type AntAB. The EPR spectrum of the D218A AntAB/anthranilate/NO sample appeared to retain a significant portion of the substrate-free component, and its overall signal intensity did not increase to the same extent as that for the wild type. The EPR spectra in Figures 6 are for Rieske-oxidized enzymes. Analogous EPR experiments on NO-reacted Rieske-reduced enzymes showed $[FeNO]^7$ EPR signals for both wild-type and D218A AntABs, and neither signal was perturbed by substrate addition (cf. Supporting Information). However, these EPR spectra also showed that NO reacted nearly completely with the reduced Rieske centers. This reaction complicates interpretation of NO binding to the proximal mononuclear sites (cf. Discussion).

"Single-Turnover" Oxidations of Wild-Type and D218A AntABs. AntAB oxidations of enzymatically reduced wild-type and D218A AntABs upon mixing with excess dioxygen

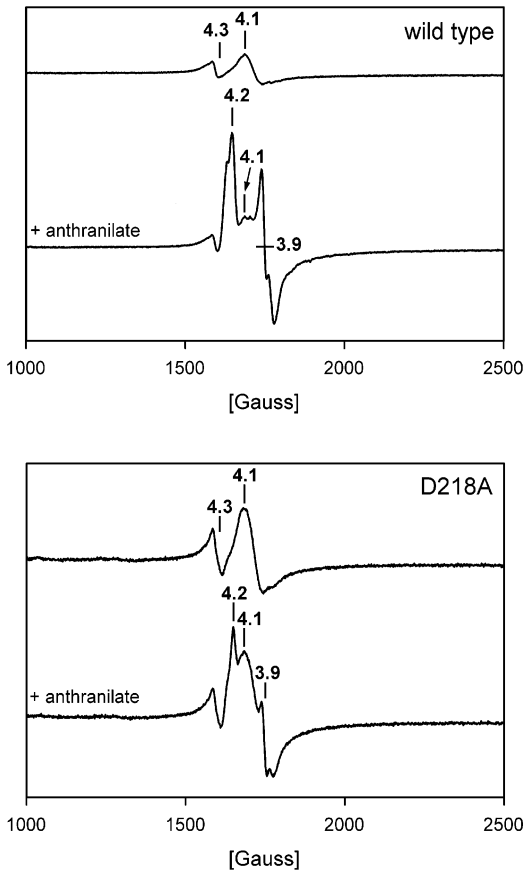

FIGURE 6: EPR spectra of nitrosyl complexes of wild-type and D218A AntAB in buffer A: top panel, wild type (165 μM $\alpha_3\beta_3$); and bottom panel, D218A (150 μM $\alpha_3\beta_3$). Within each panel, the top spectrum is of the protein without anthranilate and the bottom spectrum is the same sample but containing 1 mM anthranilate. EPR conditions: temperature, 4 K; microwave frequency, 9.59 GHz; modulation amplitude, 6.366 G; and microwave power, 2 mW.

were monitored by stopped-flow spectrophotometry. Reduction under anaerobic conditions was monitored by titration of the Rieske absorption spectrum with NADH in the presence of catalytic amounts of AntC. The time courses for reoxidation of the reduced Rieske centers upon rapid mixing with O_2-saturated buffer were then monitored by the increase in absorbance at 454 nm. The following sets of conditions were examined for both wild-type and D218A AntABs: enzymes with Fe(II)-reconstituted mononuclear sites in both the presence and absence of anthranilate, apoenzymes with anthranilate, and apoenzymes in which cobalt(II) was inserted into the mononuclear sites both with and without anthranilate. Incorporation of cobalt(II) into the mononuclear site of apoAntAB was confirmed using cobalt X-ray absorption spectroscopy (R. A. Scott, N. Cosper, D. M. Eby, E. D. Coulter, Z. Beharry, E. Neidle, and D. M. Kurtz, Jr., unpublished results). Shown in Figure 7 are the absorbance changes at 454 nm following stopped-flow mixing of O_2-saturated buffer with anaerobic solutions containing Fe(II)-reconstituted, Rieske-center-reduced wild-type or D218A AntABs and 100 μM anthranilate [a concentration which is well above saturating in assays of the wild-type enzyme activity (*15*)]. Approximately 46 and 31% (using ϵ_{454}) of the Rieske centers, respectively, were oxidized within the mixing time (~2 ms) followed by a slower phase of oxidation, which were fitted to first-order rate constants of 0.005 s^{-1} for wild-type AntAB and 0.003 s^{-1} for D218A AntAB. These fits should be considered approximate time constants only. These initial slow phases appeared to be convoluted with additional slower phases of Rieske center oxidation occurring over the course of ~30 min, which may not obey first-order kinetics. Since the pathways of these slower phases of Rieske center oxidation are obscure, and since these phases are not kinetically competent for enzymatic turnover, more detailed kinetic analyses were not undertaken. In analogous stopped-flow experiments, the initial fast phase of Rieske oxidation (i.e., within the mixing dead time) was not observed for the Fe(II)-reconstituted AntABs without anthranilate, the apoAntABs in the presence of anthranilate, or the cobalt(II)-substituted AntABs with or without anthranilate. All of these latter samples showed two phases of A_{454} increases with first-order rate constants of ~0.04 and 0.002 s^{-1} for wild-type AntAB and 0.01 and 0.004 s^{-1} for D218A AntAB followed by slower oxidation phase(s) occurring over the course of ~30 min. Samples of both wild-type and D218A AntAB that had undergone Rieske center oxidations by O_2 as described above were made anaerobic and stoichiometrically re-reduced with NADH and AntC. Remixing of these solutions with O_2-saturated buffer gave percentages of rapid and slower phases of Rieske center reoxidation similar to those described above. Analogous spectrophotometrically monitored manual mixing experiments using as-isolated (i.e., not iron-reconstituted) wild-type and D218A AntAB also yielded approximately the same percentages of fast (i.e., within the mixing time) and slower phases of Rieske center oxidation. Analogous single-turnover experiments on more concentrated AntAB solutions were monitored by EPR, as shown in Figure 8. Anaerobic, enzymatically reduced samples of Fe(II)-reconstituted wild-type and D218A AntABs showed the expected EPR signals due to the reduced Rieske centers plus the weak signal at $g = 4.3$. After 5 min reactions of the Rieske center reduced AntABs with excess O_2, the Rieske center EPR signal had lost most of its intensity, and the $g = 4.3$ signal had increased in intensity, consistent with Rieske center reoxidation and concomitant formation of some high-spin Fe(III) at the mononuclear sites. On the basis of comparisons to analogous EPR spectra of NDO and BenDO (*25*, *32*), however, the $g = 4.3$ signal intensities in Figure 8 would still account for at most a few percent of the total mononuclear iron sites. Very weak $g = 8.5$ and 5.5 signals could be due to an even smaller proportion of a second type of mononuclear high-spin ferric sites.

DISCUSSION

Effects of the Asp218 Substitutions on Properties of AntAB. On the basis of the X-ray crystal structure of NDO, Asp218 in AntAB was predicted to interact with the Rieske center across the three $\alpha-\alpha$ subunit interfaces of the $\alpha_3\beta_3$ oligomer (cf. Figure 1c). The perturbation of the UV−visible absorption spectra of the oxidized Rieske centers of the D218A, -N, and -E variant AntABs, the ~100 mV negative shift in the Rieske center reduction potential in the D218A variant, and the complete lack of dioxygenase or uncoupled oxidase activity of the variants are consistent with the expected interaction. The complete lack of activity of the D218E variant is somewhat surprising given the conservative substitution but is presumably related to the lack of iron at

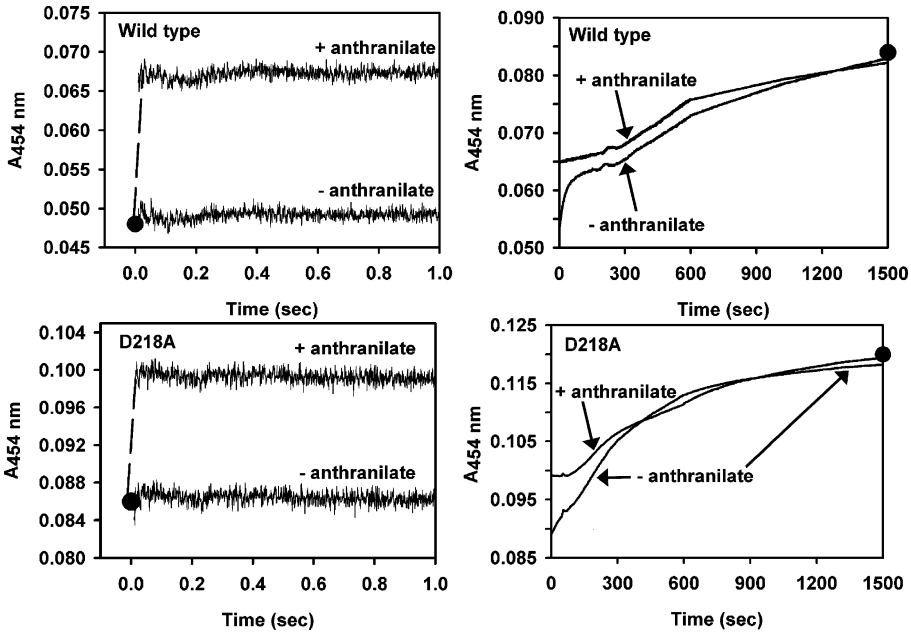

FIGURE 7: Kinetic traces monitoring the absorbance at 454 nm following stopped-flow mixing of an enzymatically reduced wild-type or D218A AntAB solution containing either no anthranilate (−anthranilate) or 200 μM anthranilate (+anthranilate) with an equal volume of a saturated O_2 solution. All solutions were in buffer A at 25 °C. Concentrations immediately after mixing were as follows: 6 μM $\alpha_3\beta_3$ for wild-type AntAB, 8 μM $\alpha_3\beta_3$ for D218A AntAB, 100 μM for anthranilate (when present), and 600 μM O_2. The left- and right-hand panels show initial portions of time courses spanning 2 s and 10 min, respectively. Circles in the left panels represent the absorbance of the reduced Rieske sites determined by stopped-flow mixing of the same solutions of reduced AntABs with the same volumes of anaerobic buffer A used for the reaction with O_2. Filled circles in the right-hand panels indicate the final absorbances of the fully reoxidized Rieske centers. The features in the time courses in the top and bottom right-hand panels at ~250 and ~50 s, respectively, are instrumental artifacts.

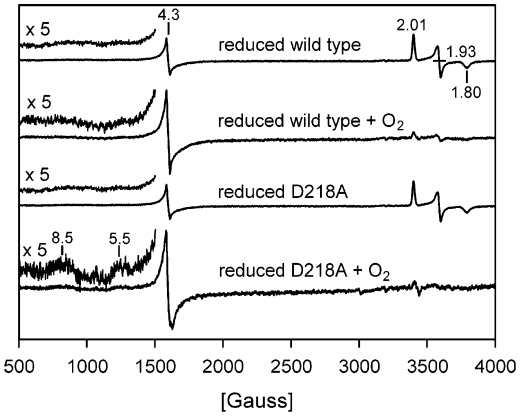

FIGURE 8: EPR spectra of one-electron enzymatically reduced wild-type AntAB (200 μM $\alpha_3\beta_3$) and D218A AntAB (125 μM $\alpha_3\beta_3$) in the presence of 10 mM anthranilate in buffer A. The notation $+O_2$ indicates spectra of the reduced enzyme solutions after mixing with an equal volume of O_2-saturated buffer A and reaction at room temperature for ~5 min. Spectral intensities for the O_2-mixed solutions were corrected for dilution. EPR conditions: temperature, 10 K; microwave frequency, 9.60 GHz; modulation amplitude, 6.366 G; and microwave power, 2 mW.

the mononuclear site. The D218A and -N variants, however, had iron contents consistent with fully occupied mononuclear sites. Since all three D218 variant AntABs retained the $\alpha_3\beta_3$ oligomeric structure of the wild-type enzyme, Asp218 cannot play an essential role in maintaining the quaternary structure of the hexamer. This observation is reminiscent of the retention of the NDO hexameric structure upon substitution of aspartate 205 (*8*).

Single-Turnover Oxidations of the Rieske Centers and NO Binding to the Mononuclear Site. The time courses of the wild-type and D218A AntAB Rieske center single-turnover oxidations by excess dioxygen are very similar to each other (cf. Figure 7). The fast phase of the Rieske center oxidations (>350 s^{-1}) far exceeds the turnover number of AntAB under our conditions (~0.7 s^{-1} from the activities listed in Table 1). This rapid phase (but not the slower phases) should, therefore, be kinetically competent for turnover in the D218A variant. However, while catechol was clearly detected as a product of the wild-type AntAB single-turnover reactions, no catechol (or related aromatic product, when monitored by HPLC) was detected under the same conditions for the D218A variant. Nevertheless, the rapid phases of the Rieske center oxidations by dioxygen were substrate-dependent in both wild-type and D218A AntABs. Since this rapid phase (≥350 s^{-1}) did not occur in either the apo or the Co(II)-substituted AntABs (with or without anthranilate), the rapid phase of Rieske center oxidation most likely occurred across the $\alpha-\alpha$ subunit interfaces via electron transfer to the mononuclear iron site during the latter's reaction with O_2 and anthranilate. The rapid phase accounted for oxidation of ~46% of wild-type and ~31% of D218A AntAB Rieske sites. These time scales and phases of Rieske center oxidations roughly parallel those observed for analogous NDO and BenDO single-turnover reactions, which notably were conducted on the dithionite-reduced oxygenase component; i.e., this behavior in our experiments is apparently not due to the presence of the reductase component (*25*, *32*). Thus, contrary to earlier suggestions (*7*, *8*), this conserved aspartate does not seem to be essential for rapid electron transfer from the reduced Rieske center to the mononuclear iron. Since both the wild-type and D218A AntABs contained their full complement of nine Fe atoms per $\alpha_3\beta_3$, the slower phases of Rieske center oxidations cannot be attributed to unoccupied mononuclear sites. The origin of the fast and slower phases may instead lie in anticooperativity; that is,

anthranilate binding to any one α subunit of a hexamer lowers either the affinity of anthranilate or the proportion of its productive binding in the other two α-subunits of the same hexamer. This explanation is also consistent with the multiple ferrous−nitrosyl EPR signals observed for wild-type AntAB in the presence of excess anthranilate (cf. Figure 6). It is noteworthy in this regard that benzoate added to BenDO in a 1:1 molar stoichiometry with iron-occupied mononuclear sites induced a conversion of the ferrous−nitrosyl EPR signal into two new signals having an intensity ratio of approximately 2:1 (*25*).

The spectral time courses (not shown) of the single-turnover Rieske center oxidations showed no evidence of distinct intermediate spectra, as might be expected if the Rieske center oxidized completely during the fast phase and underwent structural rearrangements during the subsequent slower phases. We propose that the slower Rieske center oxidation phases represent a combination of direct oxidation of the Rieske centers by molecular oxygen plus redistribution of electrons within (or between) hexamers, perhaps catalyzed by the reductase, such that the mononuclear sites become largely re-reduced. This explanation is consistent with the relatively rapid disappearance of the Rieske EPR signals from the more concentrated AntAB samples in Figure 8, and the lack of intense EPR features expected for the high-spin ferric mononuclear site upon single-turnover oxidation.[2] The analogous electron redistribution among Rieske centers was proposed to occur in NDO and BenDO (*25*, *32*). In those enzymes, a relatively intense mononuclear high-spin ferric EPR signal was observed upon single-turnover oxidations, the stability of which was proposed to arise from tight binding of the product diol near the mononuclear site. In the case of NDO, such proximal binding of the diol has been confirmed by X-ray crystallography (*6*). The relative instability of the diol product of anthranilate 1,2-dihydroxylation leads to relatively rapid formation and, apparently, dissociation of catechol. The diol product of anthranilate is, thus, unable to stabilize the ferric mononuclear site in AntDO.

Protonation State and Reduction Potential of the Rieske Center. The absorption spectrum of the oxidized AntAB Rieske center at pH 9 (cf. Figure 4) resembles that of D218A AntAB at neutral pH (cf. Figure 2), and the base-induced spectral changes in Figure 4 resemble those occurring when the oxidized Rieske center in *Thermus* Rieske ferredoxin is titrated above its pK_a of 8 (*26*). This pK_a has been attributed to ionization of a proton from one of the histidine imidazole ligands (*31*), but such behavior has not previously been reported in RDOs. As shown in Figure 1, the corresponding aspartate in NDO is within hydrogen bonding distance of one of the Rieske center histidine ligands across the three α subunit interfaces of the hexamer. This hydrogen bonding implies that the histidine ligand is protonated. The altered Rieske center absorption spectrum of D218A AntAB and of wild-type AntAB at high pH is, thus, reasonably attributed to loss of a proton from the corresponding hydrogen-bonded histidine ligand in AntAB. The other His ligand of the NDO Rieske center is similarly hydrogen-bonded across the α−α subunit interface to a glutamate carboxylate (residue E410 of the NDO α subunit) (*7*), and a sequence alignment shows that this glutamate (E432) is conserved in the α subunit of AntAB (*15*). The Rieske center in the NDO crystal structure shown in Figure 1 is thought to be in the reduced state, due to exposure of the crystals to the X-ray beam at low temperatures (*33*). These results indicate that the Rieske center His ligands in RDOs are protonated in both the oxidized and reduced states. This conclusion is borne out by a recent analysis of the pH dependence of Rieske center reduction potentials (*31*). The fact that the EPR spectrum of the reduced Rieske center of AntAB is unaffected by the D218A substitution suggests that the reduced Rieske center is also protonated in the variant. A reasonable interpretation of our results is that the Rieske center of D218A AntAB, unlike that of the wild-type protein, loses a proton from one of its histidine ligands upon oxidation at neutral pH. The loss of a proton upon oxidation is consistent with the negatively shifted reduction potential of the D218A AntAB Rieske center (*31*), and with the fact that it is the His-ligated iron of Rieske centers that undergoes oxidation and reduction (*30*). The loss of wild-type AntAB activity at pH 9 and the concomitant spectral changes of the Rieske center discussed above also lead us to associate a deprotonated Rieske center with an inactive enzyme. Since substitution of the corresponding aspartate in NDO also led to the complete loss of activity, we conclude that a protonated Rieske center, which is stabilized in the oxidized form by hydrogen bonding to a conserved aspartate residue, is essential for the dioxygenase activity of RDOs.

Lack of Coupled or Uncoupled Activity in the D218 Variant AntABs. The use of altered substrates or site-directed variants of RDOs typically leads to catalytic two-electron reduction of dioxygen via the uncoupling reaction (eq 1) with no hydroxylation of substrate (*34*, *35*).

$$\mathrm{NAD(P)H} + \mathrm{H^+} + \mathrm{O_2} \rightarrow \mathrm{H_2O_2} + \mathrm{NAD(P)^+} \qquad (1)$$

We have, in fact, previously reported that the recombinant M43K variant of AntAB exhibits anthranilate-dependent uncoupled NADH oxidase activity without substrate hydroxylation (*15*). This uncoupled activity is invariably substrate-dependent; i.e., reaction 1 has not been reported for any RDO in the absence of either substrate or substrate analogue. The D218 variant AntABs show neither coupled (Scheme 1) nor uncoupled (reaction 2) activity between pH 5.5 and 9 (encompassing the approximate stability range of these enzymes).

D218A AntAB can undergo at least two consecutive cycles of stoichiometric reduction by AntC and reoxidation of its Rieske center by dioxygen with conservation of the kinetically competent and substrate-dependent rapid oxidation phase. The complete lack of uncoupled activity in the D218 variants, implying no redox turnover of the Rieske center, is, therefore, difficult to explain. One possible explanation is that, during the first turnover of D218A AntAB, product is formed but its dissociation from the protein is sufficiently slow that it completely inhibits detectable catalytic turnover or uncoupled oxidase activity. However, no catechol (or any other product) was detected by HPLC after repeated attempts to dissociate a putative product of D218A AntAB single

[2] Relatively rapid Rieske center oxidation unaccompanied by significant mononuclear ferrous site oxidation was also observed when analogous freeze−quench single-turnover reactions of ^{57}Fe-enriched mononuclear site AntAB were monitored by Mössbauer spectroscopy (C. Krebs, Z. M. Beharry, E. D. Coulter, and D. M. Kurtz, Jr., unpublished results).

turnovers by either heat or acid denaturation, whereas catechol was readily detected for the analogous wild-type AntAB single turnovers. A more likely possibility is that the significantly lower reduction potential of the D218A AntAB Rieske center slows its reduction by NADH and AntC sufficiently to lower uncoupled activity (reaction 1), to below detectable limits. AntC contains a flavin and a ferredoxin-type (non-Rieske) [2Fe-2S] center, and the latter donates its proximal electron to the dioxygenase component (*36*). We have not measured the reduction potential of the [2Fe-2S] center in AntC, but these centers in other RDO reductases exhibit reduction potentials no lower than −200 mV versus NHE (*28*), i.e., only slightly more negative than that measured for the D218A AntAB Rieske center. On the other hand, while we have not measured the rates, reduction of the Rieske centers in both the wild-type and D218 variant AntABs occurred within the time needed to manually mix a catalytic amount of AntC with the oxidized AntAB solution containing excess NADH. These manual mixing experiments were typically conducted with 1 μM AntC and 5−30 μM AntAB hexamer. It is possible that, at the ∼10-fold lower concentrations of these enzymes used in our activity assays, the rate of Rieske center reduction by AntC cannot support detectable turnover in the D218 variants. NADH or O_2 consumption rates of less than a few micromolar per minute would not be distinguishable from background in our assays. Another possibility is that for productive turnover the protonated state of the Rieske center in all subunits of the hexamer must be maintained, which is likely to be difficult in the D218 variant AntABs. The experiments demonstrating apparently facile oxidation and reduction of the D218A Rieske center described above were conducted under non-turnover conditions on the respective reduced or oxidized protein that had been allowed to equilibrate for several minutes to several hours prior to reaction. The several minutes required for apparent deprotonation of the wild-type AntAB Rieske center following conversion to pH 9 (cf. Figure 5) implies a slow proton loss. The slowness can be attributed to burial of the Rieske center within the hydrophobic interior of the protein (*7*), and to the negatively charged, hydrogen-bonded aspartate side chains mentioned above. The Rieske center proton loss in the D218A variant may, therefore, lag behind the rapid phase of the Rieske center oxidation shown in Figure 7 under catalytic turnover conditions. Alternatively, the lack of the aspartate side chain in the D218 variants could conceivably result in relatively slow protonation of the buried Rieske center following its reduction by AntC, and, thereby, inhibit turnover.

Roles of Aspartate 218 in AntAB. Reaction of dioxygen with the mononuclear site of RDOs is gated by both substrate binding and (by analogy to nitric oxide binding) the oxidation state of the Rieske center (*25*, *32*). Subsequent rapid electron transfer from the reduced Rieske center has been proposed to generate a ferric−peroxo species (*5*, *6*, *35*), and either this or a ferryl [Fe(IV)═O(OH^-)] derived from it has been implicated as the substrate dihydroxylating species in the RDOs (*5*, *37*). The conservation of the substrate dependence for the rapid phase of Rieske center oxidation in the D218A variant, with its 100 mV negatively shifted reduction potential (measured in the absence of substrate), but unaccompanied by anthranilate dihydroxylation, argues against productive substrate gating of the Rieske center reduction potential. The fact that catechol is produced during wild-type AntAB single turnover indicates that this reaction mimics coupled catalytic turnover. Since D218A AntAB could not catalyze substrate dihydroxylation under these single-turnover conditions, substitution of the conserved aspartate must also affect substrate binding and/or the reaction of dioxygen with the mononuclear site. Although we cannot rule out the possibility that anthranilate coordinates to the mononuclear iron of AntAB, in NDO and several other RDOs (*1*), the nature of the substrate renders coordination to the mononuclear iron impossible, and substrate binding near the mononuclear site has been confirmed in the case of NDO (*6*, *38*, *39*). We, therefore, presume that anthranilate binds near but not directly to the mononuclear iron of AntAB. For wild-type AntAB, addition of anthranilate led to a significant increase in the $[FeNO]^7$ EPR signal intensity, consistent with the gating of dioxygen binding by substrate, as suggested for other RDOs (*25*, *32*). A similar increase in the EPR signal intensity upon addition of anthranilate was not apparent for the D218A variant. Furthermore, while addition of anthranilate perturbed the $[FeNO]^7$ EPR spectra of both wild-type and D218A AntAB, the EPR spectrum of the variant retained a significant portion of what appeared to be that of the substrate-free component even in the presence of 1 mM anthranilate (although we cannot rule out the possibility that this component is actually due to a second, altered substrate-bound form). A protonated Rieske center may thus promote optimal binding of both substrate and dioxygen. Due to extensive reaction of nitric oxide with the reduced Rieske centers of AntAB, we could not verify Rieske center oxidation state gating of binding of nitric oxide to the mononuclear site. The inferred increased affinity of dioxygen for the mononuclear iron site upon reduction of the Rieske centers in RDOs may originate in the >0.1 Å increase in the average Fe−NHis bond length, which has been observed in AntAB by EXAFS (*40*). The resulting structural and electronic rearrangement could be transmitted to the mononuclear iron site and/or the substrate binding site across the α−α subunit interface via the hydrogen-bonded aspartate (*39*). For both AntAB and NDO, substitution of this aspartate led to essentially complete inhibition of substrate dihydroxylation (*8*). This conserved aspartate residue must, therefore, be crucial not only for maintaining the protonation state and redox potential of the Rieske center but also for substrate dihydroxylation at the mononuclear iron site of RDOs.

ACKNOWLEDGMENT

We thank Mike Clay for assistance in obtaining the EPR spectra and Professor Mike Johnson for helpful discussions concerning the Rieske center.

SUPPORTING INFORMATION AVAILABLE

EPR spectra of enzymatically reduced wild-type AntAB−nitrosyl complexes and enzymatically reduced D218A AntAB−nitrosyl complexes. This material is available free of charge via the Internet at http://pubs.acs.org.

REFERENCES

1. Nam, J. W., Nojiri, H., Yoshida, T., Habe, H., Yamane, H., and Omori, T. (2001) New classification system for oxygenase components involved in ring-hydroxylating oxygenations, *Biosci., Biotechnol., Biochem. 65*, 254−263.

2. Gibson, D. T., and Parales, R. E. (2000) Aromatic hydrocarbon dioxygenases in environmental biotechnology, *Curr. Opin. Biotechnol. 11*, 236−243.
3. Bertini, I., Cremonini, M. A., Ferretti, S., Lozzi, I., Luchinat, C., and Viezolli, M. S. (1996) Arene hydroxylases: metalloenzymes catalysing dioxygenation of aromatic compounds, *Coord. Chem. Rev. 151*, 145−160.
4. Butler, C. S., and Mason, J. R. (1997) Structure−function analysis of the bacterial aromatic ring-hydroxylating dioxygenases, *Adv. Microb. Physiol. 38*, 47−84.
5. Que, L., Jr., and Ho, R. Y. N. (1996) Dioxygen activation by enzymes containing mononuclear non-heme iron active sites, *Chem. Rev. 96*, 2607−2624.
6. Karlsson, A., Parales, J. V., Parales, R. E., Gibson, D. T., Eklund, H., and Ramaswamy, S. (2003) Crystal structure of naphthalene dioxygenase: side-on binding of dioxygen to iron, *Science 299*, 1039−1042.
7. Kauppi, B., Lee, K., Carredano, E., Parales, R. E., Gibson, D. T., Eklund, H., and Ramaswamy, S. (1998) Structure of an aromatic-ring-hydroxylating dioxygenase-naphthalene 1,2-dioxygenase, *Structure 6*, 571−586.
8. Parales, R. E., Parales, J. V., and Gibson, D. T. (1999) Aspartate 205 in the catalytic domain of naphthalene dioxygenase is essential for activity, *J. Bacteriol. 181*, 1831−1837.
9. Sayle, R., and Milner-White, E. J. (1995) RASMOL: biomolecular graphics for all, *Trends Biochem. Sci. 20*, 374−376.
10. Carredano, E., Karlsson, A., Kauppi, B., Choudhury, D., Parales, R. E., Parales, J. V., Lee, K., Gibson, D. T., Eklund, H., and Ramaswamy, S. (2000) Substrate binding site of naphthalene 1,2-dioxygenase: functional implications of indole binding, *J. Mol. Biol. 296*, 701−712.
11. Bundy, B. M., Campbell, A. L., and Neidle, E. L. (1998) Similarities between the *antABC*-encoded anthranilate dioxygenase and the benABC-encoded benzoate dioxygenase of *Acinetobacter* sp. strain ADP1, *J. Bacteriol. 180*, 4466−4474.
12. Neidle, E. L., Shapiro, M. K., and Ornston, L. N. (1987) Cloning and expression in *Escherichia coli* of *Acinetobacter calcoaceticus* genes for benzoate degradation, *J. Bacteriol. 169*, 5496−5503.
13. Yamaguchi, M., and Fujisawa, H. (1982) Subunit structure of oxygenase component in benzoate-1,2-dioxygenase system from *Pseudomonas arvilla* C-1, *J. Biol. Chem. 257*, 12497−12502.
14. Altier, D. J., Fox, B. G., Münck, E., and Lipscomb, J. D. (1993) EPR And Mössbauer characterization of benzoate 1,2-dioxygenase from *P. putida*, *J. Inorg. Biochem. 51*, 300.
15. Eby, D. M., Beharry, Z. M., Coulter, E. D., Kurtz, D. M., Jr., and Neidle, E. L. (2001) Characterization and evolution of anthranilate 1,2-dioxygenase from *Acinetobacter* sp. strain ADP1, *J. Bacteriol. 183*, 109−118.
16. Schagger, H., and von Jagow, G. (1987) Coomassie blue-sodium dodecyl sulfate-polyacrylamide gel electrophoresis for direct visualization of polypeptides during electrophoresis, *Anal. Biochem. 166*, 368−379.
17. Sambrook, J., Fritsch, E. F., and Maniatis, T. (1990) *Molecular cloning: a laboratory manual*, 2nd ed., Cold Spring Harbor Laboratory Press, Plainview, NY.
18. Ausubel, F. A., Brent, R., Kingston, R. E., Moore, D. D., Seidman, J. G., Smith, J. A., and Struhl, K. (1990) *Current Protocols in Molecular Biology*, Green Publishing and Wiley-Interscience, New York.
19. Neidle, E. L., and Ornston, L. N. (1986) Cloning and expression of *Acinetobacter calcoaceticus* catechol 1,2-dioxygenase structural gene *catA* in *Escherichia coli*, *J. Bacteriol. 168*, 815−820.
20. Hewitt, L. F. (1950) *Oxidation-Reduction Potentials in Bacteriology and Biochemistry*, E. & S. Livingston, Ltd., Edinburgh, Scotland.
21. Eidsness, M. K., Burden, A. E., Richie, K. A., Kurtz, D. M., Jr., Scott, R. A., Smith, E. T., Ichiye, T., Beard, B., Min, T., and Kang, C. (1999) Modulation of the redox potential of the [Fe(SCys)$_4$] site in rubredoxin by the orientation of a peptide dipole, *Biochemistry 38*, 14803−14809.
22. Eidsness, M. K., Burden, A. E., Richie, K. A., Kurtz, D. M., Jr., Scott, R. A., Smith, E. T., Ichiye, T., Beard, B., Min, T., and Kang, C. (2000) Modulation of the redox potential of the [Fe(SCys)$_4$] site in rubredoxin by the orientation of a peptide dipole (correction), *Biochemistry 39*, 626.
23. Alberty, R. A. (1998) Calculation of standard transformed formation properties of biochemical reactants and standard apparent reduction potentials of half reactions, *Arch. Biochem. Biophys. 358*, 25−39.
24. Shanley, M. S., Neidle, E. L., Parales, R. E., and Ornston, L. N. (1986) Cloning and expression of *Acinetobacter calcoaceticus catBCDE* genes in *Pseudomonas putida* and *Escherichia coli*, *J. Bacteriol. 165*, 557−563.
25. Wolfe, M. D., Altier, D. J., Stubna, A., Popescu, C. V., Münck, E., and Lipscomb, J. D. (2002) Benzoate 1,2-dioxygenase from *Pseudomonas putida*: single turnover kinetics and regulation of a two-component Rieske dioxygenase, *Biochemistry 41*, 9611−9626.
26. Kuila, D., and Fee, J. A. (1986) Evidence for a redox-linked ionizable group associated with the [2Fe-2S] cluster of *Thermus* Rieske protein, *J. Biol. Chem. 261*, 2768−2771.
27. Correll, C. C., Batie, C. J., Ballou, D. P., and Ludwig, M. L. (1992) Phthalate dioxygenase reductase: a modular structure for electron transfer from pyridine nucleotides to [2Fe-2S], *Science 258*, 1604−1610.
28. Rosche, B., Fetzner, S., Lingens, F., Nitschke, W., and Riedel, A. (1995) The 2Fe2S centres of the 2-oxo-1,2-dihydroquinoline 8-monooxygenase from *Pseudomonas putida* 86 studied by EPR spectroscopy, *Biochim. Biophys. Acta 1252*, 177−179.
29. Riedel, A., Fetzner, S., Rampp, M., Lingens, F., Liebl, U., Zimmermann, J. L., and Nitschke, W. (1995) EPR, electron spin−echo envelope modulation, and electron nuclear double resonance studies of the 2Fe2S centers of the 2-halobenzoate 1,2-dioxygenase from *Burkholderia* (*Pseudomonas*) *cepacia* 2CBS, *J. Biol. Chem. 270*, 30869−30873.
30. Link, T. A. (1999) in *Advances in Inorganic Chemistry* (Sykes, A. G., and Cammack, R., Eds.) pp 83−157, Academic Press, New York.
31. Zu, Y., Fee, J. A., and Hirst, J. (2001) Complete thermodynamic characterization of reduction and protonation of the bc(1)-type Rieske [2Fe-2S] center of *Thermus thermophilus*, *J. Am. Chem. Soc. 123*, 9906−9907.
32. Wolfe, M. D., Parales, J. V., Gibson, D. T., and Lipscomb, J. D. (2001) Single turnover chemistry and regulation of O_2 activation by the oxygenase component of naphthalene 1,2-dioxygenase, *J. Biol. Chem. 276*, 1945−1953.
33. Karlsson, A., Parales, J. V., Parales, R. E., Gibson, D. T., Eklund, H., and Ramaswamy, S. (2000) The reduction of the Rieske iron−sulfur cluster in naphthalene dioxygenase by X-rays, *J. Inorg. Biochem. 78*, 83−87.
34. Lee, K. (1999) Benzene-induced uncoupling of naphthalene dioxygenase activity and enzyme inactivation by production of hydrogen peroxide, *J. Bacteriol. 181*, 2719−2725.
35. Twilfer, H., Sandfort, G., and Bernhardt, F. H. (2000) Substrate and solvent isotope effects on the fate of the active oxygen species in substrate-modulated reactions of putidamonooxin, *Eur. J. Biochem. 267*, 5926−5934.
36. Karlsson, A., Beharry, Z. M., Eby, D. M., Coulter, E. D., Neidle, E. L., Kurtz, D. M., Jr., Eklund, H., and Ramaswamy, S. (2002) X-ray crystal structure of benzoate 1,2-dioxygenase reductase from *Acinetobacter* sp. strain ADP1, *J. Mol. Biol. 318*, 261−272.
37. Wolfe, M. D., and Lipscomb, J. D. (2003) Hydrogen peroxide-coupled cis-diol formation catalyzed by naphthalene 1,2-dioxygenase, *J. Biol. Chem. 278*, 829−835.
38. Yang, T. C., Wolfe, M. D., Neibergall, M. B., Mekmouche, Y., Lipscomb, J. D., and Hoffman, B. M. (2003) Substrate binding to NO-ferro-naphthalene 1,2-dioxygenase studied by high-resolution Q-band pulsed ^{2}H-ENDOR spectroscopy, *J. Am. Chem. Soc. 125*, 7056−7066.
39. Yang, T. C., Wolfe, M. D., Neibergall, M. B., Mekmouche, Y., Lipscomb, J. D., and Hoffman, B. M. (2003) Modulation of substrate binding to naphthalene 1,2-dioxygenase by Rieske cluster reduction/oxidation, *J. Am. Chem. Soc. 125*, 2034−2035.
40. Cosper, N. J., Eby, D. M., Kounosu, A., Kurosawa, N., Neidle, E. L., Kurtz, D. M., Jr., Iwasaki, T., and Scott, R. A. (2002) Redox-dependent structural changes in archaeal and bacterial Rieske-type [2Fe-2S] clusters, *Protein Sci. 11*, 2969−2973.

BI035385N